Chinese Journal of Chemical Engineering 53 (2023) 289–299

Contents lists available at ScienceDirect

Chinese Journal of Chemical Engineering

journal homepage: www.elsevier.com/locate/CJChE

Full Length Article

Electrospinning organic solvent resistant preoxidized poly(acrylonitrile) nanofiber membrane and its properties

Zhiwei Du [1,2], Jinxue Cheng [1,2], Qinglin Huang [1,2,*], Mingxing Chen [3,*], Changfa Xiao [4]

[1] State Key Laboratory of Separation Membranes and Membrane Processes/National Center for International Joint Research on Separation Membranes, Tianjin 300387, China
[2] Department of Material Science and Engineering, Tiangong University, Tianjin 300387, China
[3] College of Textile and Garments, Hebei University of Science and Technology, Shijiazhuang 050018, China
[4] Fiber Materials Research Center, Shanghai University of Engineering Science, Shanghai 201620, China

ARTICLE INFO

Article history:
Received 17 September 2021
Received in revised form 23 January 2022
Accepted 24 January 2022
Available online 26 March 2022

Keywords:
Poly(acrylonitrile) (PAN)
Preoxidation
Nanofiber membrane
Solvent resistance
Oil/water separation

ABSTRACT

A high performance preoxidized poly(acrylonitrile) (O-PAN) nanofiber membrane with excellent solvent resistance, thermal stability and flexibility was fabricated by the preoxidation of electrospun PAN nanofiber membrane. The performance of resultant O-PAN nanofiber membrane was optimized by altering the PAN concentration and preoxidation temperature. The results showed that the O-PAN nanofiber membrane which made from PAN concentration of 14% (mass) and preoxidation temperature of 250.0 °C have a more optimal comprehensive performance. In the long-term separation test of SiO_2 particle (1 μm) in DMAc suspension, the permeate flux of O-PAN nanofiber membrane stabilized at 227.91 $L{\cdot}m^{-2}{\cdot}h^{-1}$ (25 °C, 0.05 MPa) while the SiO_2 rejection above 99.6%, which showed excellent solvent resistance and separation performance. In order to further explore the application of the O-PAN nanofiber membrane, the O-PAN nanofiber membrane was treated with fluoride and used in oil/water separation process. The O-PAN nanofiber membrane after hydrophobic treatment showed excellent hydrophobicity and good oil/water separation performance with the permeate flux about 969.59 $L{\cdot}m^{-2}{\cdot}h^{-1}$ while the separation efficiency above 96.1%. The O-PAN nanofiber membrane exhibited a potential application prospect in harsh environment separation.

1. Introduction

As an energy-saving and environment-friendly separation technology, membrane technology has been successfully applied in many fields, such as water treatment [1–3], new energy resource [4,5], gas separation [6,7], pervaporation [8–10], and organic solvent separation [11,12]. With the rapid development of membrane technology, the requirement of membrane's performance is getting higher and higher, such as membrane's chemical and thermal stability, solvent resistance, permeability, service life, and so on. Especially, the industrial separation processes involving high temperature, acid or alkaline base, organic solvents and other harsh environments have more stringent requirements for membrane [13–15]. Therefore, developing the membrane with excellent chemical and thermal stability, solvent-resistant, flexible and lower cost is meaningful.

Poly(acrylonitrile) (PAN) is a highly commercialized polymeric membrane material which is widely used in microfiltration, ultrafiltration, and nanofiltration owing to its good comprehensive properties. However, the PAN suffers poor solvent stability in most polar solvent (such as DMF, DMAc, NMP) owing to the strong polar group of C≡N [16]. Moreover, the thermal stability of PAN is also weak. However, it is well known that PAN fibers are the precursor of high-quality carbon fiber, which experiences three processes, namely preoxidation, carbonization and graphitization. Preoxidation process is the heat treatment of PAN fibers in air atmosphere, during which a complex chemical changes in terms of cyclization, dehydrogenation, oxidation, and crosslinking will occur at this stage, and a stable trapezoidal chemical structure can be finally formed [17–19]. Inspired by the preoxidation treatment of PAN fiber, there are many literatures about preoxidation of PAN porous membrane aiming to improve the membrane's performance. For example, Tsai *et al.* [20] successfully prepared a NMP-insoluble preoxidized PAN hollow fiber membrane and applied it to the pervaporation of NMP/H_2O mixtures. Li *et al.* [21] successfully fabricated a kind of preoxidized self-crosslinked TiO_2/PAN hybrid

* Corresponding authors.
E-mail addresses: huangqinglin@tiangong.edu.cn (Q. Huang), mxchen1990@163.com (M. Chen).

https://doi.org/10.1016/j.cjche.2022.01.030
1004-9541/

membrane, which showed excellent thermal stability and solvent resistant. Zhang *et al.* [22] optimized the microstructure of the PAN nanofiltration membrane by preoxidation treatment. The $CaCl_2$ rejection of the peroxidation PAN nanofiltration membrane was about 99.9% with the feed concentration of 50 mg·L^{-1} and pH value of 3. The preoxidized PAN membrane prepared by Li *et al.* [23] presented excellent thermal and chemical stability, especially in DMAc with high temperature of 116.1 °C. Therefore, the preoxidation treatment of PAN membrane can effectively improve the membrane's performance.

In this work, a kind of preoxidized PAN (O-PAN) nanofiber membrane was prepared by the preoxidation of electrospun PAN nanofiber membrane. The effects of PAN concentration and preoxidation temperature on the structure and performance of O-PAN nanofiber membrane were investigated, respectively. Then, the O-PAN nanofiber membrane was treated with fluoride and used in oil/water separation process. The prepared O-PAN nanofiber membrane exhibited excellent solvent resistance, thermal stability and flexibility, which showed a potential application prospect in harsh environment separation.

2. Experimental

2.1. Materials

Poly(acrylonitrile) (PAN, molecular weight = 250000 Da) was purchased from Macklin Biochemical Technology Co., Ltd., Shanghai, China. *N*,*N*-dimethylformamide (DMF, Analytical Reagent) and *N*,*N*-dimethylacetamide (DMAc, Analytical Reagent) were purchased from Kermel Chemical Reagent Co., Ltd., Tianjin, China. SiO_2 (1 μm) particles was provided by Shanghai Pantian Nano Materials Co., Ltd, (Shanghai, China). The comparative sample of poly(vinylidene fluoride) (PVDF) membrane was prepared by non-solvent induced phase inversion (NIPS) method in our laboratory (15% (mass) PVDF, 6% (mass) DOP, 3% (mass) LiCl, 76% (mass) DMAc). Trimethoxy (1H,1H,2H,2H-heptadecafluorodecyl) silane ($C_{13}H_{13}F_{17}O_3Si$, named 17-FAS) was purchased from Aladdin Industrial Co., Ltd., Shanghai, China. Hexane was purchased from Kermel Chemical Reagent Co., Ltd., Tianjin, China.

2.2. Membrane fabrication

Firstly, the homogeneous PAN spinning solution was prepared with the composition detail tabulated in Table 1. While the PAN solution was electrospun at a positive voltage of 23 kV and negative voltage of 5 kV, a spinning distance of 15 cm and a fluid flow rate of 1.5 ml·h^{-1}. The relative humidity and temperature were fixed at values of (25±5)% and (23 ± 2) °C, respectively.

Finally, the O-PAN nanofiber membrane was obtained by the preoxidation of PAN nanofiber membrane. The details of the preoxidation were tabulated in Table 2. The schematic diagram of preparing PAN and O-PAN nanofiber membrane was shown in Fig. 1. In order to enhance the hydrophobic properties of the membrane, 2 g 17-FAS was mixed with 98 g hexane and the O-PAN membrane was immersed in the above solution. After soaked for 24 h, the membrane was taken out and heat treated at 120 °C for 2 h in muffle furnace to complete the hydrophobic modification. The schematic diagram of hydrophobic treatment was shown in Fig. 2.

Table 1
The code and composition of the PAN spinning solution

Membrane code	PAN/% (mass)	DMF/% (mass)
M-1	10	90
M-2	12	88
M-3	14	86
M-4	16	84

2.3. Membrane characterization

The membrane morphologies were observed by scanning electron microscopy (FESEM, Hitachi S-4800, Japan) after gold spraying.

The elemental analysis of the membrane surface were measured by energy dispersive spectrometer (EDAX, APOLLO XL, USA).

Membrane's surface chemistry composition was verified by Fourier transform infrared spectroscopy (FTIR, Nicolet iS50) in the range of 4000–500 cm^{-1} under a transmittance mode.

The thermal degradation behavior of the nanofiber membrane was monitored by simultaneous thermal analysis instrument (TG-DSC, STA 449F5, Germany) under nitrogen atmosphere from 20 °C to 800 °C at a heating rate of 10 °C·min^{-1}.

Dynamic mechanical analyzer (DMA242E, Germany) was used to test the dynamic modulus and damping of the membrane under the condition of programmed temperature rise. The PAN and O-PAN membranes were cut into 0.5 cm × 5 cm (wide × length) strips, and then fixed on the stretching fixture. The absolute amplitude was set as 30 μm, the maximum dynamic force was 0.5 N, the additional static force was 0.1 N, the frequency was 1 Hz, and the heating rate was 3 °C·min^{-1}.

Static water contact angle measurements were tested using an optical contact angle meter (DSA100, KRUSS, Germany) by the sessile drop method of water. A droplet of water with a volume of 0.2 μl was deposited on the membrane surface. Five different spots were measured for each sample.

The mean pore size and pore size distribution were measured using a capillary flow porometer (3H-2000 PB, Beishide Instrument Technology Co., Ltd., China) and the membrane porosity was determined by the gravimetric method with *n*-butyl alcohol as a wetting liquid, which is determined from Eq. (1):

$$\varepsilon = \frac{\omega_2 - \omega_1}{A \times d \times \rho} \times 100\% \quad (1)$$

where ω_2 is the mass of wetted membrane (g), ω_1 is the mass of the dry membrane (g), A is the area of the membrane (cm^2), d is the average thickness of the membrane (cm), and ρ is the density of *n*-butyl alcohol (ρ = 0.811 g·cm^{-3}). The mechanical strength of nanofiber membrane was analyzed at room temperature using an electronic tensile tester (JBDL-200 N, Yangzhou Jingbo Instrument, China) at a stretching rate of 5 mm·min^{-1}. The samples were cut into 0.5 cm × 5 cm (wide × length) strips, and each sample was tested five times.

The PAN and O-PAN nanofiber membranes were cut into an appropriate size and weighed using an electronic balance, then immersed in organic solvent (DMF). After soaking for 7 days, the nanofiber membrane was dried in a vacuum oven to constant mass, and weighed again to calculate the mass loss. The number of samples in each group was 5, and the values were averaged.

2.4. Separation performance

2.4.1. SiO_2 particle separation

The obtained PAN and O-PAN membranes were used to separate the SiO_2 dispersion (SiO_2 particle size 1 μm, dispersed in water and also DMAc with the concentration of 0.1 g·L^{-1}). The concentration of SiO_2 before and after filtration was measured by turbidimeter. The schematic diagram of the particle separation was shown in Fig. 3.

Table 2
The program temperature of preoxidation process

Membrane code	Start temperature/°C	Heating rate/°C·min^{-1}	Maximum temperature/°C	Holding time/h	Cooling rate/°C·min^{-1}
M-3-190	30.0 ± 1.0	1.0 ± 0.1	190.0 ± 1.0	2.0 ± 0.1	10 ± 2.0
M-3-220	30.0 ± 1.0	1.0 ± 0.1	220.0 ± 1.0	2.0 ± 0.1	10 ± 2.0
M-3-250	30.0 ± 1.0	1.0 ± 0.1	250.0 ± 1.0	2.0 ± 0.1	10 ± 2.0

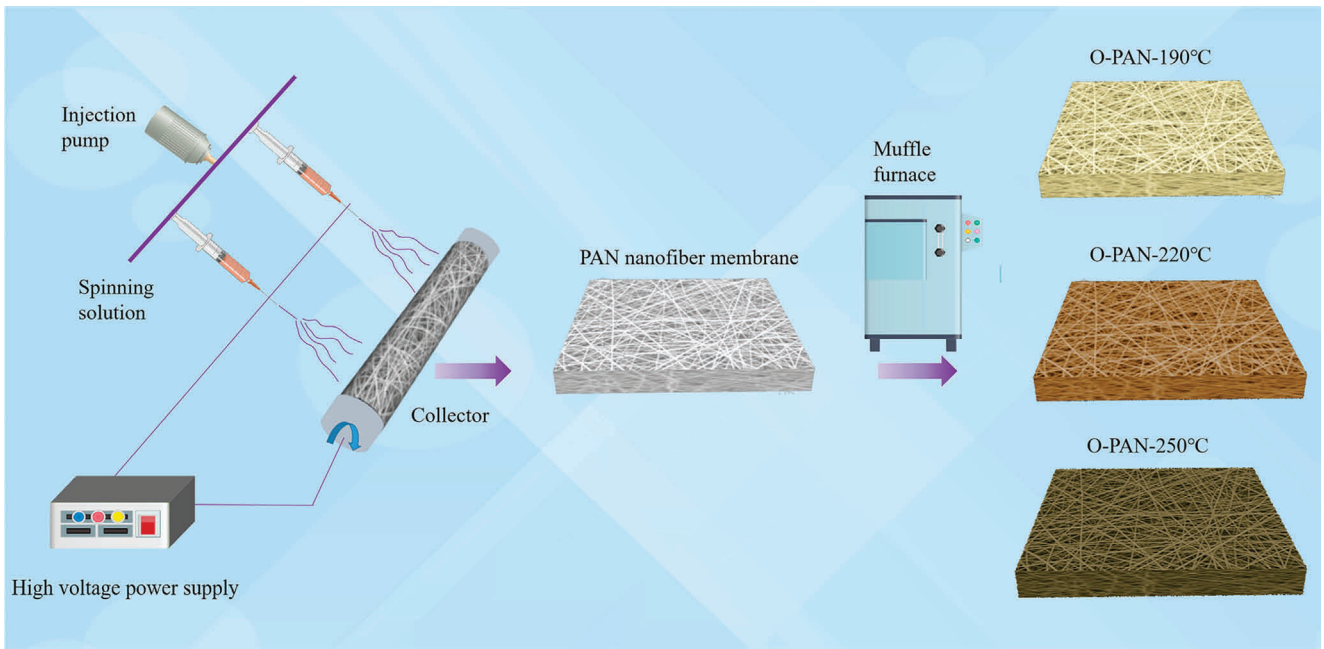

Fig. 1. Schematic diagram of preparing PAN and O-PAN nanofiber membrane.

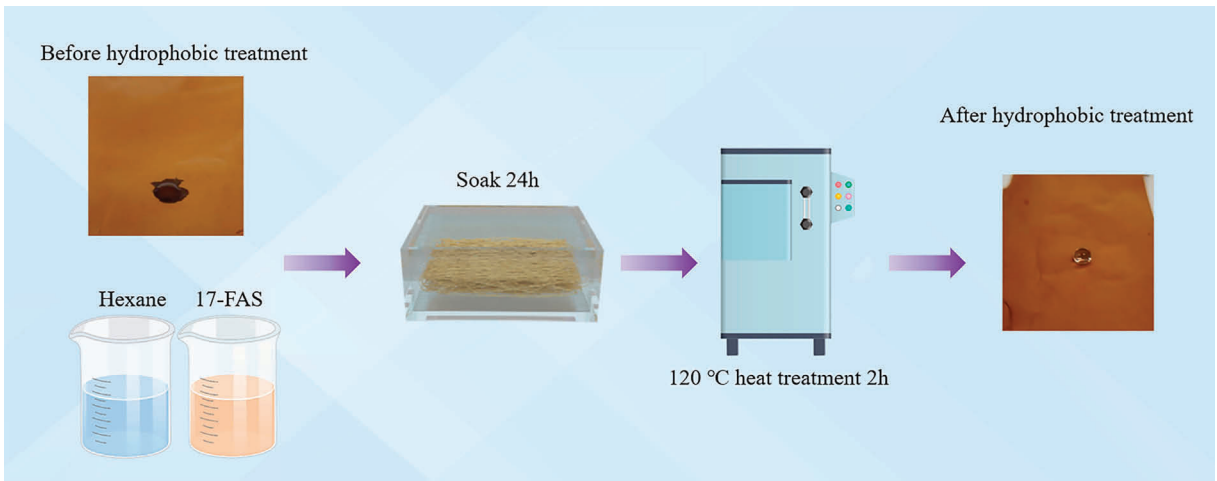

Fig. 2. Schematic diagram of hydrophobic treatment.

The permeate flux was calculated according to Eq. (2):

$$J = \frac{V}{A \times t} \tag{2}$$

where J is the permeate flux (L·m^{-2}·h^{-1}); V, A and t is the volume of permeation (L), the available area of membrane (m^2) and the testing time (h), respectively.

The separation efficiency of the membrane was calculated by Eq. (3):

$$R = \left(1 - \frac{C_p}{C_f}\right) \times 100\% \tag{3}$$

where R is the rejection (%), and C_f and C_p are the concentration of SiO_2 in the feed and permeate solution, respectively.

2.4.2. Oil/water separation

The oil/water mixture (1:1, v/v) was composed of distilled water dyed by methylene blue while kerosene dyed by Sundan

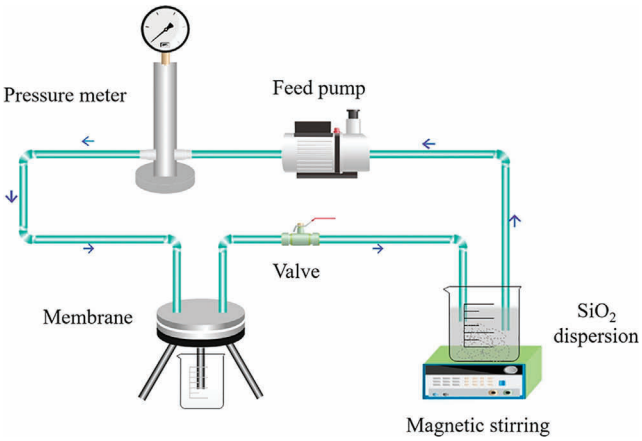

Fig. 3. Schematic diagram of particle separation test (operation pressure 0.05 MPa).

III. The oil/water mixture was poured into the tilted solvent filter, took the form of negative pressure (−0.01 MPa) to separate oil and water. The permeate flux was calculated according to Eq. (2). The oil/water separation efficiency was calculated according to Eq. (4):

$$\eta = \frac{V_1 - V_2}{V_3} \times 100\% \tag{4}$$

where η is the oil/water separation efficiency (%), V_1 is the volume of collected oil after separation (ml), V_2 is the volume of collected water after separation (ml), V_3 is the volume of oil before separation (ml).

After running for 5 min, the membrane was removed and cleaned with alcohol for the next test of oil/water separation experiment. The experiment was repeated for 10 cycles, and the flux recovery rate was calculated as follows:

$$\mathrm{FRR} = \frac{J_1}{J_0} \times 100\% \tag{5}$$

where FRR is the flux recovery rate (%), J_1 is the flux after cleaning ($L{\cdot}m^{-2}{\cdot}h^{-1}$), J_0 is the original flux ($L{\cdot}m^{-2}{\cdot}h^{-1}$).

3. Results and Discussion

3.1. Membrane morphology

Fig. 4 showed the SEM images of the electrospun PAN nanofiber membrane with different PAN concentrations. It can be found that the fiber diameter increased gradually with the increase of PAN concentration. The beadlike structure can be clearly observed from Fig. 4(a) and (b), when the PAN concentration was 10% (mass) and 12% (mass). While the fiber diameter became obviously larger and the adhesion appeared (Fig. 4(d)) as PAN concentration increased to 16% (mass). The PAN nanofiber with 14% (mass) concentration exhibited good morphology with neither beadlike structure nor obvious adhesion (Fig. 4(c)). Therefore, the 14% (mass) PAN nanofiber membrane (M-3) was used in the following peroxidation process.

Fig. 5 showed the EDX, WCA, SEM images and digital photos of PAN nanofiber membrane and O-PAN nanofiber membrane with

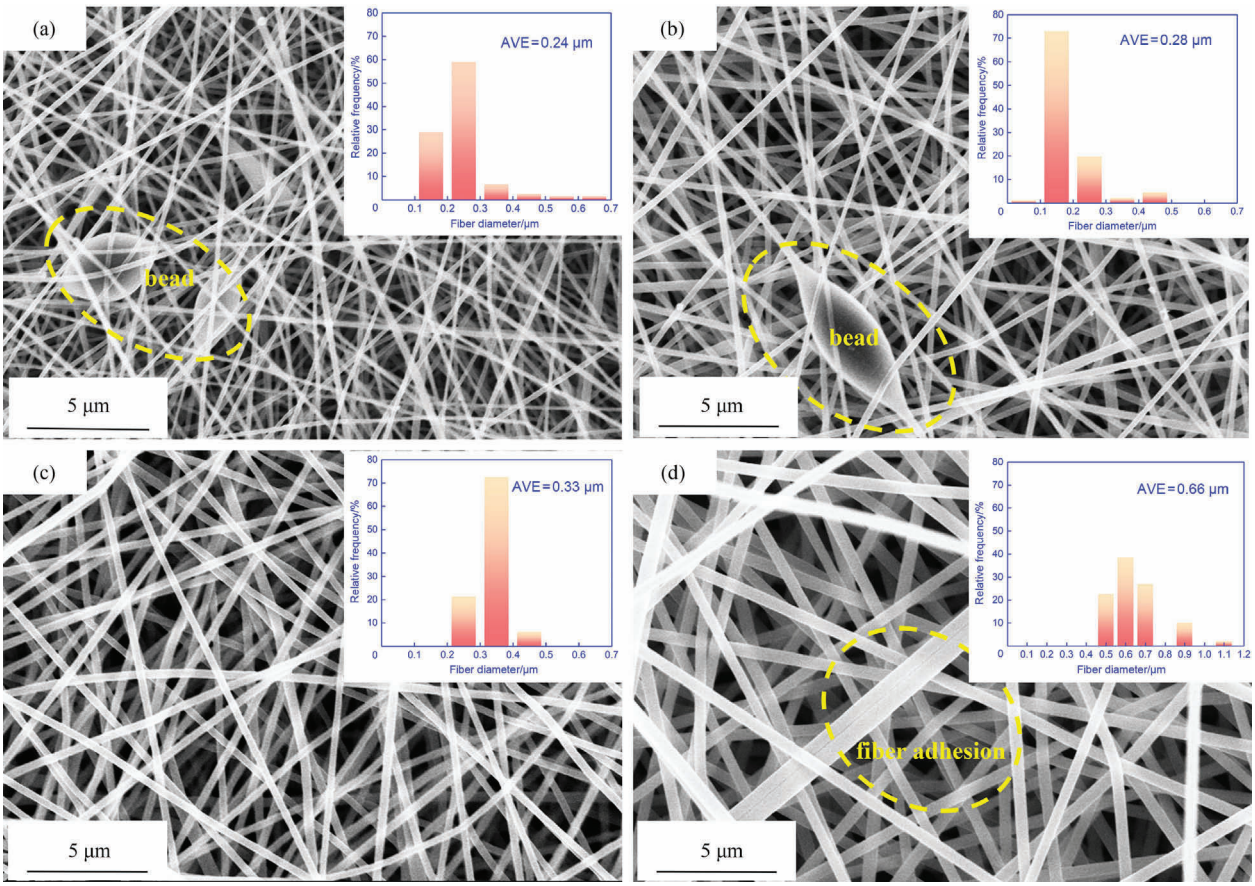

Fig. 4. SEM of membrane with different PAN concentrations: (a) M-1, (b) M-2, (c) M-3, (d) M-4.

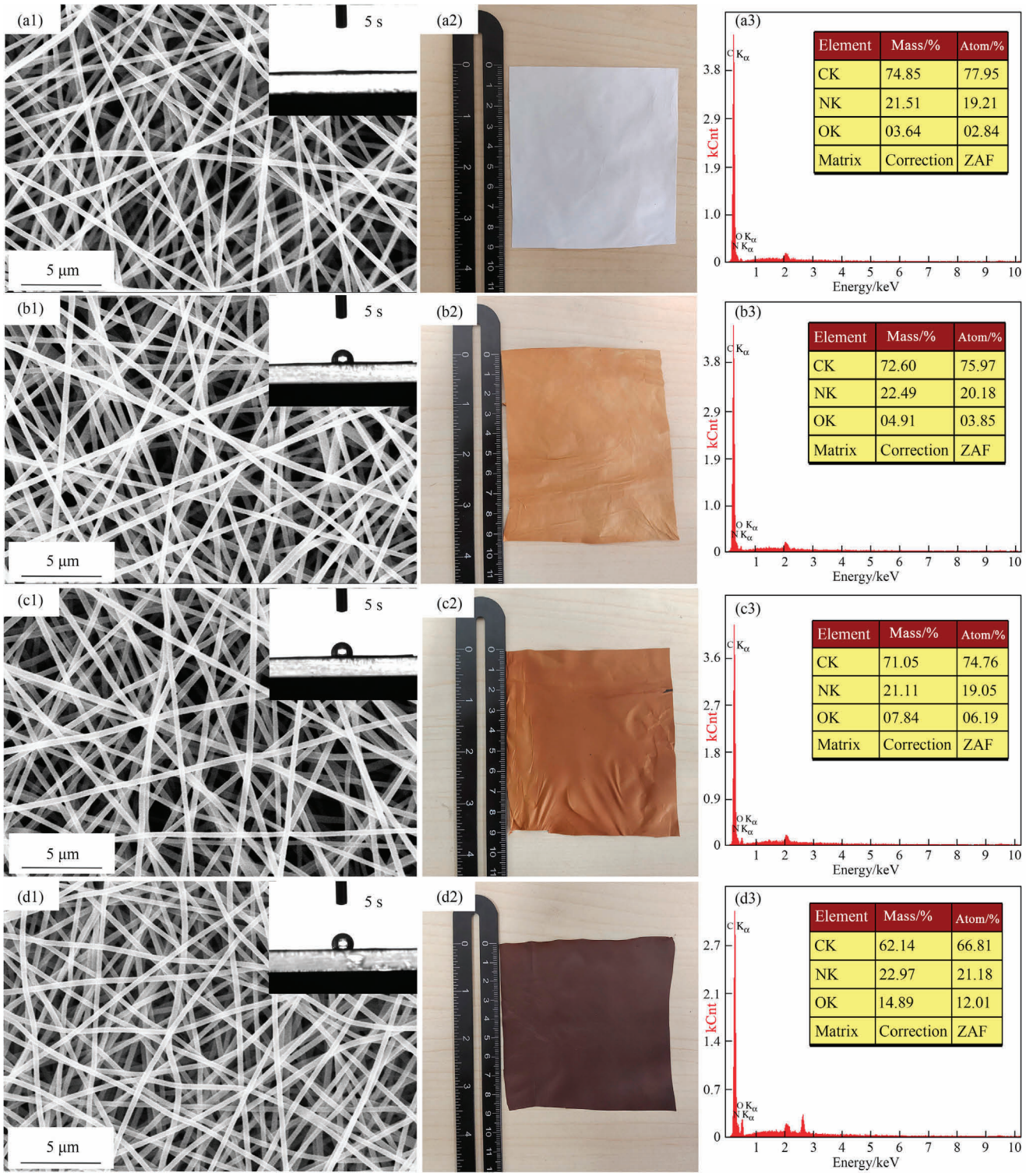

Fig. 5. EDX, SEM, WCA and digital photos of PAN and O-PAN nanofiber membrane: (a) M-3, (b) M-3-190, (c) M-3-220, (d) M-3-250.

different preoxidation temperature. As can be seen from Fig. 5(a1)–(d1), all the O-PAN nanofiber membrane maintained the fiber structure, although the color changes during the peroxidation process (Fig. 5(a2)–(d2)). It can be found that the content of element C gradually decreased while element O increased with the increase of preoxidation temperature from Fig. 5(a3)–(d3). Combined with WCA images, the PAN membrane showed strong hydrophilicity owing to the hydrophilic group —C≡N, while the O-PAN membrane showed hydrophobicity in a short time because of the cyclization of group —C≡N after peroxidation process.

3.2. Membrane porosity and pore size

The effects of preoxidation temperature on the porosity and pore size of O-PAN nanofiber membrane were shown in Fig. 6. It can be found that the porosity and pore size of O-PAN nanofiber

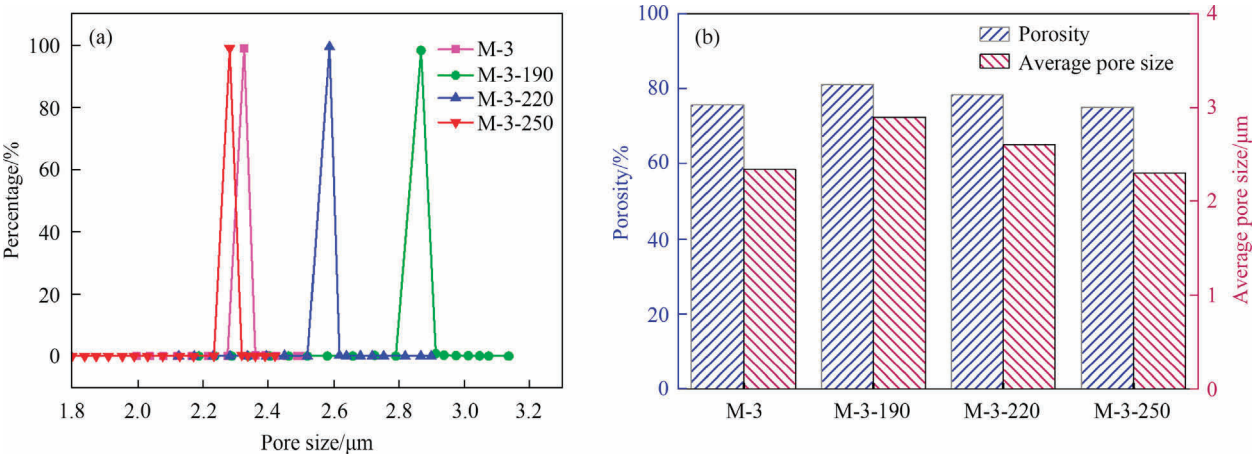

Fig. 6. Effects of preoxidation temperatures on (a) pore size distribution and (b) average pore size and porosity of nanofiber membrane.

membrane increased at first and then decreased as the preoxidation temperature increased. At lower preoxidation temperature, the PAN nanofiber became fluffy when heated, causing a slightly larger pore size. As the temperature increased, the nanofiber membrane would shrink due to the improved cyclization degree of molecular chain. This phenomenon also can be seen from Fig. 5 (a1)–(d1). Therefore, the membrane pore size obviously increased at first and then decreased.

3.3. Membrane structure and properties

3.3.1. Chemical composition and thermal behavior

The chemical reactions in peroxidation process were shown in Fig. 7(a). Stabilization preoxidation of PAN membranes is usually carried out by heat treatment in the temperature of 180–300 °C. The macromolecules cross-link together through the chemical bonds and make PAN membranes with good chemical stability after peroxidation treatment. The FTIR results (Fig. 7(b)) showed the changes of the chemical composition of the PAN and O-PAN nanofiber membrane. It can be found that, the peaks of —CH_2 (2940, 1450 cm^{-1}) and —C≡N (2245 cm^{-1}) which belong to PAN were gradually weakened owing to the dehydrogenation and cyclization reactions during the peroxidation process. Meanwhile, the signal intensities of —C=N (1590 cm^{-1}), —C=C— (1370 cm^{-1}) and —CH (810 cm^{-1}) belong to O-PAN were significantly enhanced, which demonstrated the occurrence of the cyclization and dehydrogenation reaction of PAN [24,25]. When the preoxidation temperature raised to 250 °C, the signal intensities of —C≡N, —CH_2 could be hardly observed, while the signal strength of —C=N, —C=C— and —CH reached a very high degree.

Fig. 8 showed the TGA curves of PAN and O-PAN nanofiber membrane. There were two obvious mass-loss of the PAN nanofiber membrane, which one was the water vaporization or low molecular decomposition near 100 °C. The other mass-loss was owing to the reaction of dehydrogenation and decomposition around 280 °C, which was the same as O-PAN nanofiber membrane. Moreover, all the O-PAN nanofiber membrane showed good thermal stability until 280 °C. Especially for M-3-250, the mass-loss begun at about 332.7 °C, thermal stability improved with the increase of preoxidation temperature. It can also be seen that the mass loss rate of the membrane decreased with the increased of the preoxidation temperature, and the mass residual of M-3-250

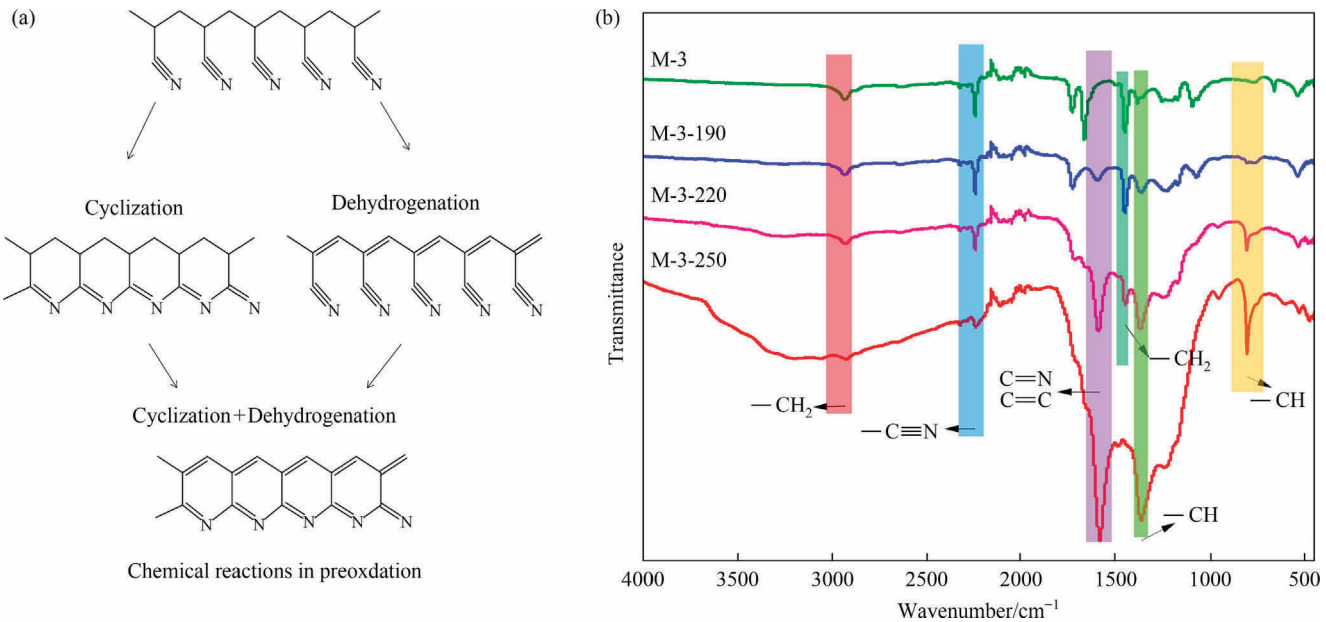

Fig. 7. Chemical composition of PAN and O-PAN nanofiber membrane: (a) chemical reactions, (b) FT-IR spectra.

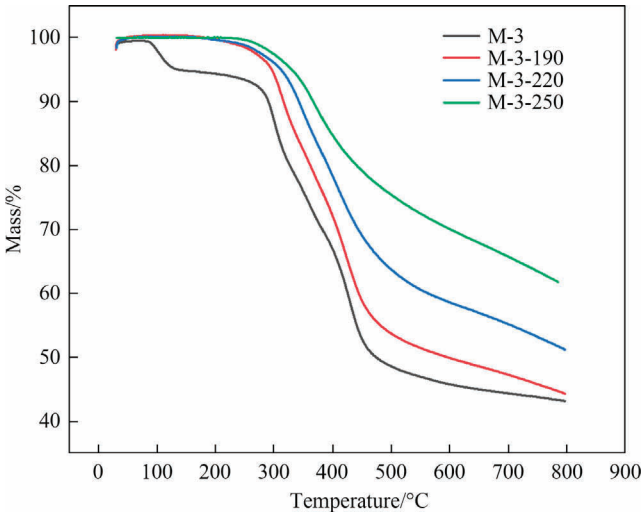

Fig. 8. TGA curves of PAN and O-PAN nanofiber membrane.

Table 3
Mechanical strength of PAN and O-PAN nanofiber membrane

Membrane code	Membrane thickness/μm	Breaking strength/MPa	Breaking elongation/%
M-3	97.3 ± 8.2	3.6 ± 0.4	20.2 ± 4.1
M-3-190	84.4 ± 6.1	5.4 ± 0.5	13.4 ± 2.2
M-3-220	85.3 ± 8.5	5.5 ± 0.3	4.3 ± 1.1
M-3-250	88.5 ± 7.2	5.6 ± 0.1	3.1 ± 0.1

was significantly higher than that of M-3. This was due to the formation of stable heat-resistant trapezoidal structure in the preoxidation process, which can be relatively stable in the subsequent carbonization process, thus increased the yield of carbon fiber, further indicated that the preoxidation treatment improved the thermal stability of the membrane [26–28].

3.3.2. Mechanical strength and DMA analysis

The mechanical performance of nanofiber membrane was tabulated in Table 3. It can be found that there was an obvious enhancement in breaking strength from 3.65 MPa (M-3) to 5.62 MPa (M-3-250), while the breaking elongation decreased with peroxidation temperature incensement. After preoxidation, the molecular structure of PAN changed from single bond long chain to trapezoidal structure, which resulted in the increase of the breaking strength. When the PAN membrane was preoxidized, the entangled chains relaxed first, then contracted, and finally rearranged into ordered structures. This would weaken the membranes' flexibility significantly. Therefore, the breaking elongation of O-PAN nanofiber membrane decreased with peroxidation temperature incensement.

Fig. 9 showed the DMA results of PAN and O-PAN nanofiber membrane. It can be seen that the internal friction peak gradually moved to low temperature, and the corresponding glass transition temperature decreased from 111.1 °C (M-3) to 89.4 °C (M-3-250) with the increase of preoxidation temperature. Meanwhile, the tanδ corresponding to the internal friction peak decreased from 0.228 (M-3) to 0.070 (M-3-250). This was caused by the cyclization and dehydrogenation reaction of PAN in the process of preoxidation. A higher binding degree of —C≡N of PAN would lead to a

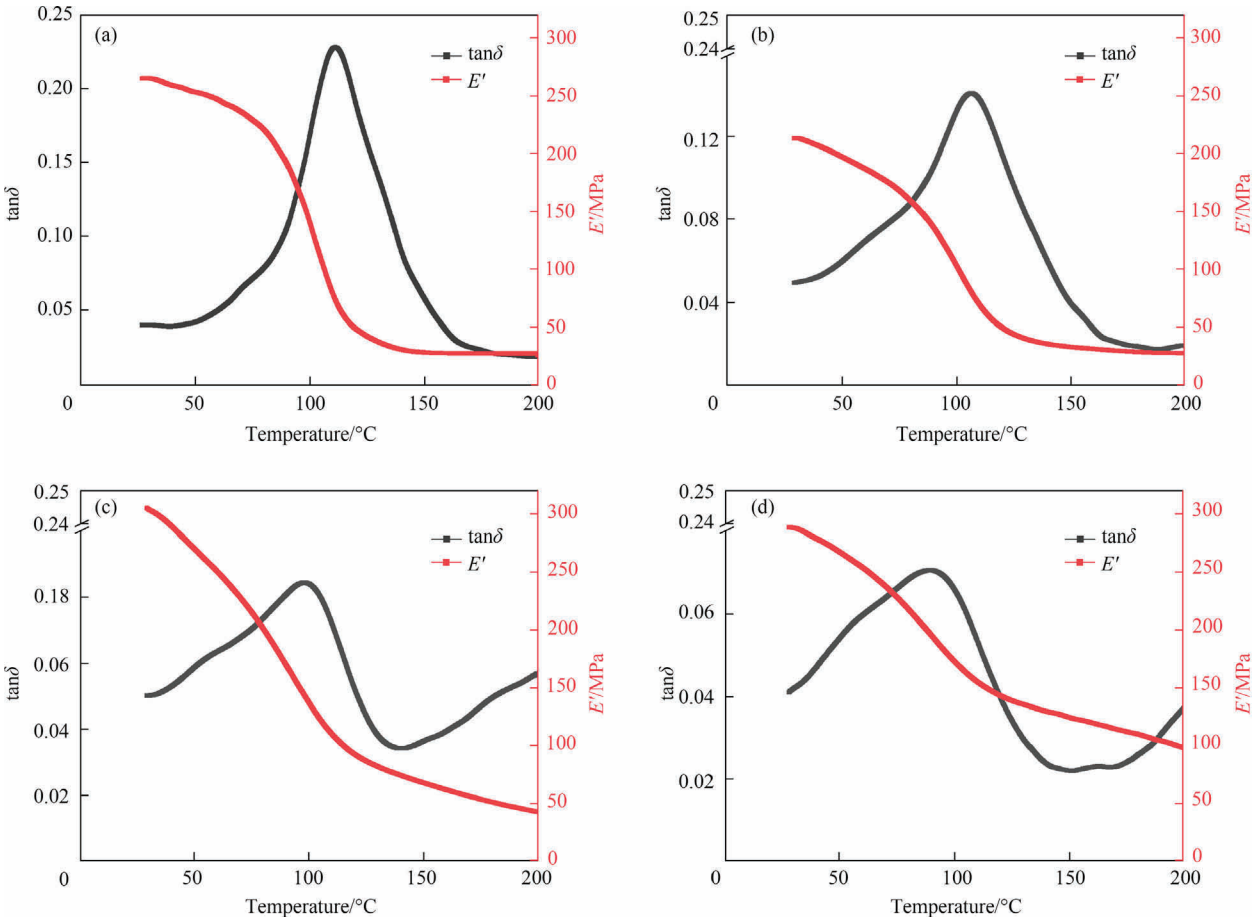

Fig. 9. DMA of PAN and O-PAN nanofiber membrane: (a) M-3, (b) M-3-190, (c) M-3-220, (d) M-3-250.

smaller size of relaxed chain segment, and further induced the lower required energy for the movement of the chain segment. Therefore, the internal friction peak moved to the low temperature, and the corresponding tanδ value decreased gradually.

3.4. Membrane performance

3.4.1. Chemical stability

Table 4 showed the mass changes of different samples after soaked in organic solvent (DMF). It can be seen that both PAN and PVDF membranes were completely dissolved in DMF. While the mass change of O-PAN membrane was very small, especially M-3-250. The mass change of M-3-250 was almost zero as the chemical structure has changed significantly after preoxidization. The cyclation reaction had obtained the stable trapezoidal structure, so the stability of the membrane in DMF solvent was significantly improved.

Fig. 10 showed the SEM morphologies of membranes before and after soaked in DMF. After soaked in DMF, PAN and PVDF membranes completely dissolved in a short time, showed poor resistance to DMF solvent. As shown in Fig. 10(b2), the M-3-190 nanofiber membrane had obvious dissolved, the nanofiber obviously adhered together. Relatively in Fig. 10(c2)–(d2), the membranes were not dissolved, and the nanofibers had no adhesion phenomenon, the overall excellent surface morphology was maintained. Based on the mass changed and surface morphology changed of the membrane, the M-3-250 showed excellent solvent resistance in organic solvent (DMF).

3.4.2. Separation performance

Fig. 11 showed the results of SiO_2 particle separation performance in water solution and organic solvent. In water solution, the rejection rate of SiO_2 particle was more than 99.0% by the PAN and O-PAN membranes. The PAN membrane would be dissolved by DMAc solvent, therefore the SiO_2 particle couldn't be separated by PAN nanofiber membrane. By contrast, the O-PAN membrane showed good separation performance with the permeate flux stabilized at 227.91 $L{\cdot}m^{-2}{\cdot}h^{-1}$ while the SiO_2 rejection above 99.6%.

Fig. 12(a) showed the changes of membrane surface hydrophobicity with time before and after hydrophobic treatment. It can be seen that the water droplet can infiltrate the membrane before hydrophobic treatment in a short time, while the membrane after hydrophobic treatment showed excellent hydrophobicity. Fig. 12(b) showed the oil/water separation process. It can be seen that the red kerosene was successfully collected in the conical flask below through the membrane, and the blue distilled water was trapped by the membrane. The hydrophobically modified O-PAN membrane showed good oil/water separation performance. Fig. 12(c) showed the permeate flux and separation efficiency. The permeate flux gradually decreased from 1591.11 $L{\cdot}m^{-2}{\cdot}h^{-1}$ (M-3-190) to 969.59 $L{\cdot}m^{-2}{\cdot}h^{-1}$ (M-3-250). Meanwhile, the oil/water separation efficiency gradually increased from 92.0% (M-3-190) to 96.1% (M-3-250). From the previous SEM, pore size distribution and FTIR, we know that with the increase of preoxidation temperature, the pore size of the membrane gradually decrease, and the number of hydrophilic group also decrease. Combined with the

Table 4
The mass changes of samples after soaked for 7 days

Membrane samples	M-3	M-3-190	M-3-220	M-3-250	PVDF
Mass change/%	×	−1.2 ± 0.1	−0.6 ± 0.1	—	×

× indicates the membrane was completely dissolved by solvent; — indicates the mass change of the membrane is almost zero.

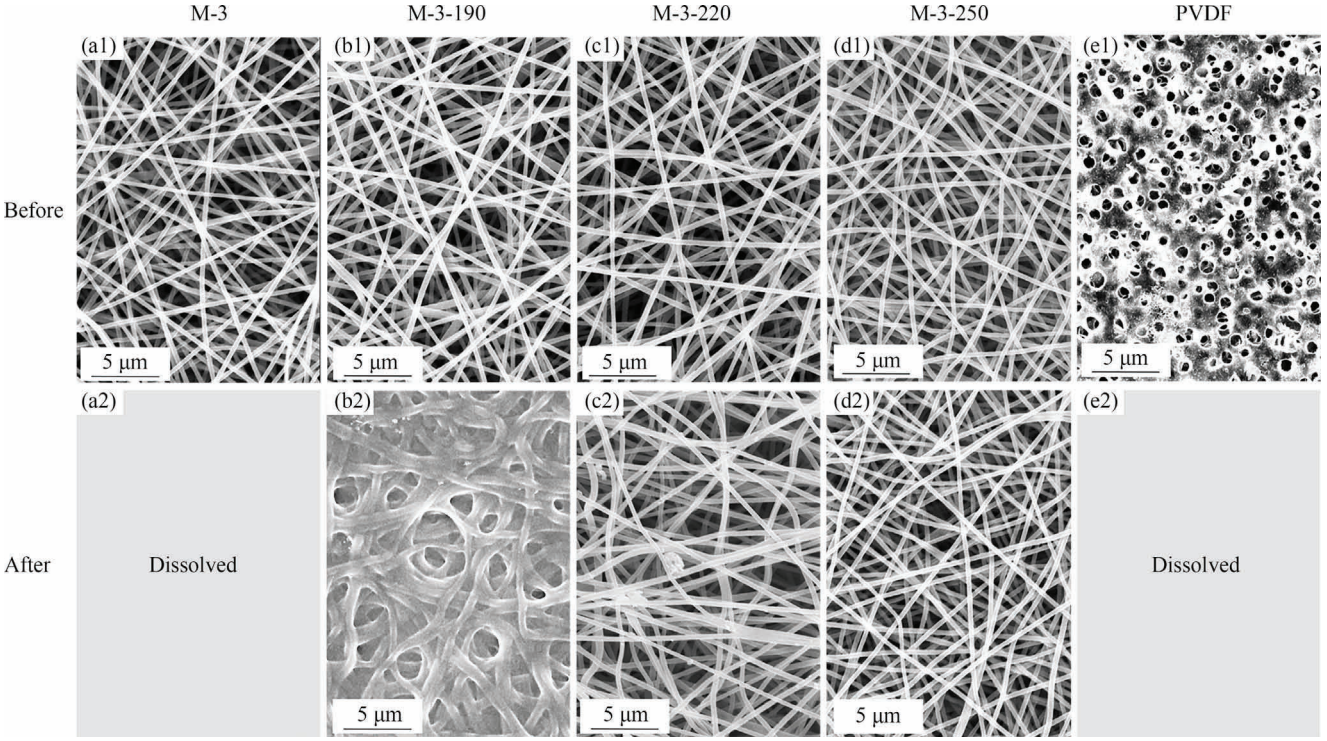

Fig. 10. SEM of membranes before and after soaked in DMF: (a) M-3, (b) M-3-190, (c) M-3-220, (d) M-3-250, (e) PVDF.

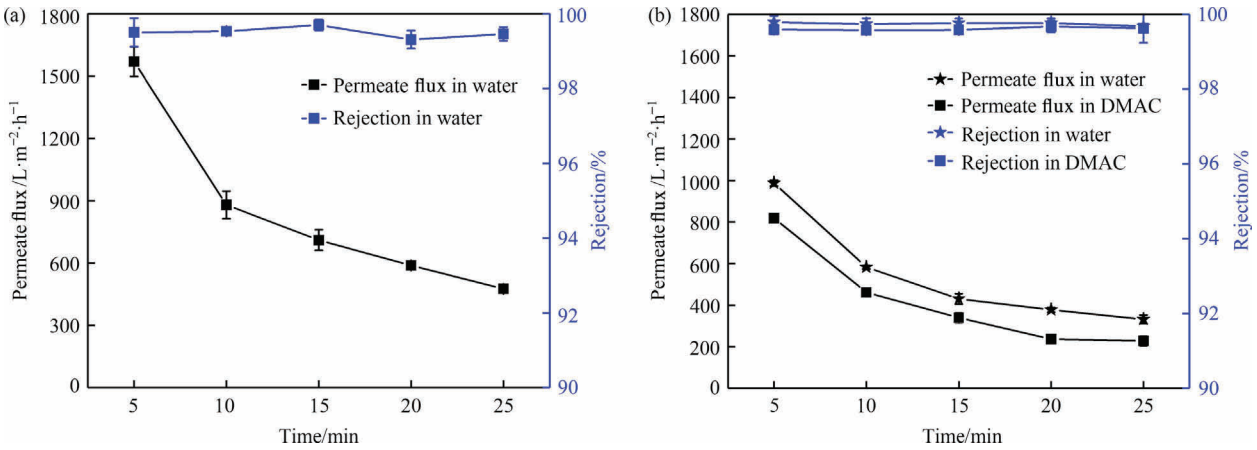

Fig. 11. The separation performance for SiO_2 particle solution of the nanofiber membranes: (a) M-3, (b) M-3-250.

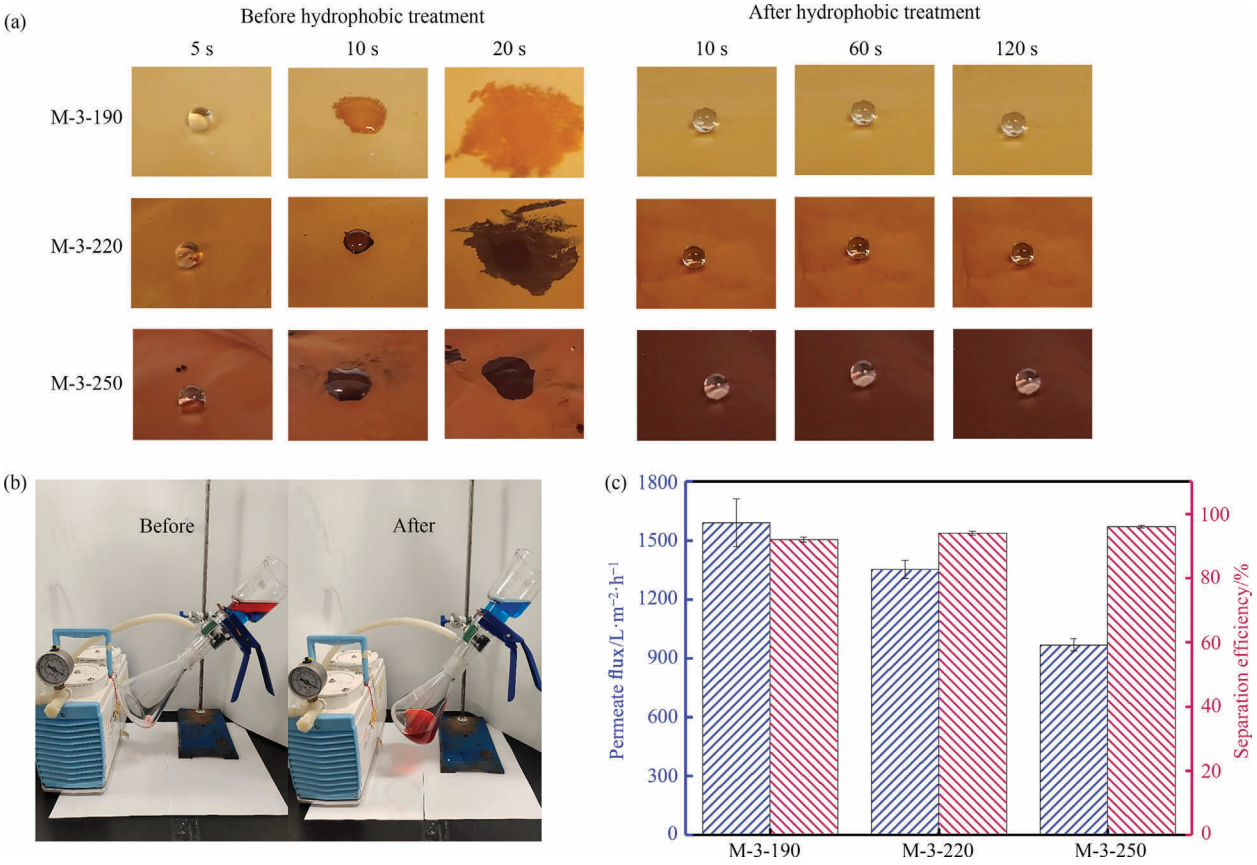

Fig. 12. The effects of hydrophobic treatment on wettability of O-PAN nanofiber membrane (a) and oil/water separation performance (b) and (c).

subsequent hydrophobic treatment leaded to the decrease of permeate flux and the improvement of separation efficiency.

Fig. 13 showed the results of oil flux recovery rate and oil/water separation efficiency after alcohol cleaning. It can be found that oil flux recovery rates and separation efficiency of the hydrophobic O-PAN nanofiber membrane were kept over 95% and 92%, respectively. There was no significant decline after 10 cycles. The results showed that the hydrophobic modification of O-PAN nanofiber membrane was superior stable.

As mentioned above, the obtained O-PAN membranes showed good separation performance of SiO_2 particle in DMAc solvent with the permeate flux stabilized at 227.91 $L{\cdot}m^{-2}{\cdot}h^{-1}$ and the SiO_2 rejection above 99.6%, and excellent oil/water separation performance with the permeate flux about 969.59 $L{\cdot}m^{-2}{\cdot}h^{-1}$ while the separation efficiency above 96.1% after hydrophobic treatment. To highlight the superior performances, we conducted a comparison of the performances between O-PAN nanofiber membrane and other reported membrane (Table 5). Compared with other reported membranes, they can only separate substances in water systems, O-PAN nanofiber membrane showed excellent organic solvent resistance and can complete particle separation in organic solvent system.

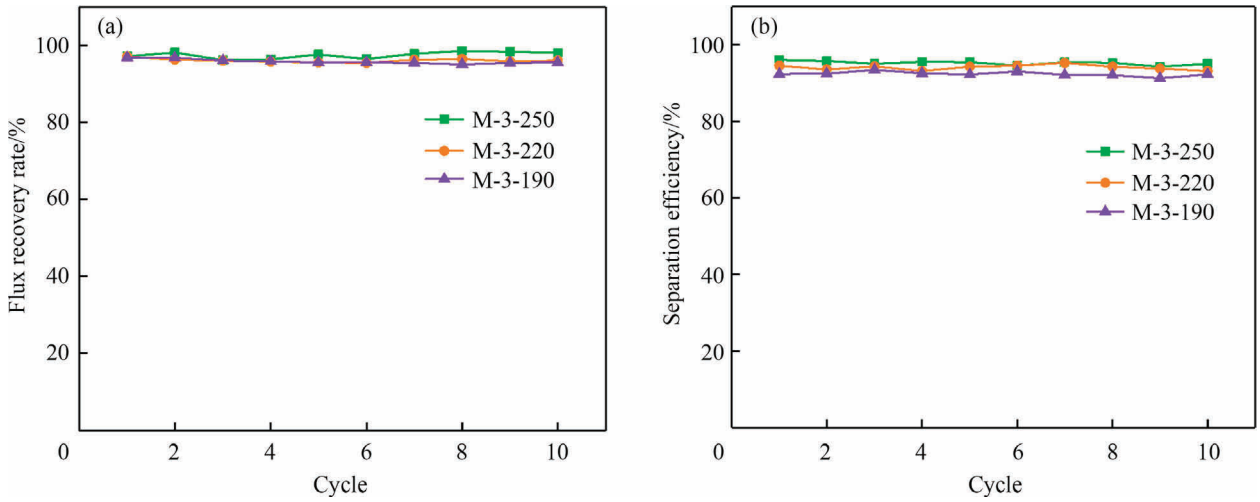

Fig. 13. Oil flux recovery rate (a) and oil/water separation efficiency (b) over 10 cycles.

Table 5
Comparison of the performances between the electrospinning membrane in this study and others reported in the literature

Membrane composition	Wettability	Rejection material	Solvent	Tested pressure/ MPa	Permeate flux/ $L{\cdot}m^{-2}{\cdot}h^{-1}$	Rejection/ %	Ref
PES/PET	Hydrophobic	PS particle (1 μm)	Water	0.20	—	98.0	[29]
PVDF/GO	Hydrophilic	Kaolin solution	Water	0.10	~250.0	99.8	[30]
PAN/PET	Hydrophilic	Polybead carboxylate microspheres (1 μm)	Water	—	192.0	99.0	[31]
PAN/TEOS	Hydrophilic	PS particle (1 μm)	Water	—	—	~95.0	[32]
PAN/JCNs	Hydrophilic	SiO_2 particle (7–40 nm)	Water	Self-weight	—	99.0	[33]
O-PAN	Hydrophilic	SiO_2 particle (1 μm)	DMAc	0.05	227.9	99.6	This work
	Hydrophobic	Oil/Water	Oil/ Water	−0.01	969.6–1591.1	92.0–96.1	

Note: PES—Polyether sulfone; PET—Poly(ethylene terephthalate); PVDF—Poly (vinyldene fluoride); GO—Graphene oxide; TEOS—Tetraethyl orthosilicate; JCNs—Jute cellulose nanowhiskers.

4. Conclusions

A high performance O-PAN nanofiber membrane was fabricated by the preoxidation treatment of electrospun PAN nanofiber membrane. The optimized O-PAN nanofiber membrane was made from PAN concentration of 14% (mass) and preoxidized temperature at 250 °C. The obtained O-PAN membranes not only showed good thermal and solvent resistance, but also good separation performance of SiO_2 particle in DMAc solvent with the permeate flux stabilized at 227.91 $L{\cdot}m^{-2}{\cdot}h^{-1}$ and the SiO_2 rejection above 99.6%. The prepared O-PAN nanofiber membrane showed good application prospect in the harsh environment separation. In addition, the membrane after hydrophobic treatment showed excellent hydrophobicity and good oil/water separation performance with the permeate flux about 969.59 $L{\cdot}m^{-2}{\cdot}h^{-1}$ while the separation efficiency above 96.1%.

Declaration of Competing Interest

The authors declare that they have no known competing financial interests or personal relationships that could have appeared to influence the work reported in this paper.

Acknowledgements

This work was supported by the Science and Technology Plans of Tianjin (18PTSYJC00170), the Young Elite Scientists Sponsorship Program by China Association for Science and Technology (YESS20160168). The Analytical & Testing Center of Tiangong University was appreciated.

Supplementary Material

Supplementary data to this article can be found online at https://doi.org/10.1016/j.cjche.2022.01.030.

References

[1] L. Song, Q.L. Huang, Y. Huang, R.F. Bi, C.F. Xiao, An electro-thermal braid-reinforced PVDF hollow fiber membrane for vacuum membrane distillation, *J. Membr. Sci.* 591 (2019) 117359.
[2] J. Gao, T.S. Chung, Influence of contaminants in glycerol/water mixtures during post-treatment on physicochemical properties and separation performance of air-dried membranes, *J. Membr. Sci.* 572 (2019) 223–229.
[3] Z.H. Yang, G.L. Zhang, F.N. Liu, Q. Meng, Physicochemical characteristics of hollow fiber structured packings in isopropanol/water distillation, *Ind. Eng. Chem. Res.* 49 (22) (2010) 11594–11601.
[4] C. Shi, J.H. Dai, X. Shen, L.Q. Peng, C. Li, X. Wang, P. Zhang, J.B. Zhao, A high-temperature stable ceramic-coated separator prepared with polyimide binder/Al_2O_3 particles for lithium-ion batteries, *J. Membr. Sci.* 517 (2016) 91–99.
[5] S.R. Park, Y.C. Jung, W.K. Shin, K.H. Ahn, C.H. Lee, D.W. Kim, Cross-linked fibrous composite separator for high performance lithium-ion batteries with enhanced safety, *J. Membr. Sci.* 527 (2017) 129–136.
[6] X.F. Hu, W.H. Lee, J.Y. Bae, J.Y. Zhao, J.S. Kim, Z. Wang, J.L. Yan, Y.M. Lee, Highly permeable polyimides incorporating Tröger's base (TB) units for gas separation membranes, *J. Membr. Sci.* 615 (2020) 118533.
[7] M. Minelli, M. Giacinti Baschetti, D.T. Hallinan Jr, N.P. Balsara, Study of gas permeabilities through polystyrene-block-poly(ethylene oxide) copolymers, *J. Membr. Sci.* 432 (2013) 83–89.

[8] H.Z. Zeng, S.J. Liu, J. Wang, Y.B. Li, L. Zhu, M. Xu, C.W. Wang, Hydrophilic SPEEK/PES composite membrane for pervaporation desalination, *Sep. Purif. Technol.* 250 (2020) 117265.
[9] W.Z. Ma, T.Y. Li, C. Jiang, P. Zhang, L. Deng, R. Xu, Q. Zhang, J. Zhong, H. Matsuyama, Effect of chain structure on the solvent resistance in aprotic solvents and pervaporation performance of PMDA and BTDA based polyimide membranes, *J. Membr. Sci.* 584 (2019) 216–226.
[10] H.A. Tsai, Y.S. Ciou, C.C. Hu, K.R. Lee, D.G. Yu, J.Y. Lai, Heat-treatment effect on the morphology and pervaporation performances of asymmetric PAN hollow fiber membranes, *J. Membr. Sci.* 255 (1–2) (2005) 33–47.
[11] Z.Y. Zhou, Y.X. Hu, Q. Wang, B.X. Mi, Carbon nanotube-supported polyamide membrane with minimized internal concentration polarization for both aqueous and organic solvent forward osmosis process, *J. Membr. Sci.* 611 (2020) 118273.
[12] Y. Zhao, Y.B. Qiu, Z.H. Mai, E. Ortega, J.N. Shen, C.J. Gao, B. van der Bruggen, Symmetrically recombined nanofibers in a high-selectivity membrane for cation separation in high temperature and organic solvent, *J. Mater. Chem. A* 7 (34) (2019) 20006–20012.
[13] C. Li, W.J. Sun, Z.D. Lu, X.W. Ao, S.M. Li, Ceramic nanocomposite membranes and membrane fouling: A review, *Water Res.* 175 (2020) 115674.
[14] B. Pulido, S. Chisca, S.P. Nunes, Solvent and thermal resistant ultrafiltration membranes from alkyne-functionalized high-performance polymers, *J. Membr. Sci.* 564 (2018) 361–371.
[15] Z. Yang, Y. Zhou, Z.Y. Feng, X.B. Rui, T. Zhang, Z.E. Zhang, A review on reverse osmosis and nanofiltration membranes for water purification, *Polymers* 11 (8) (2019) 1252.
[16] V. Lachat, V. Varshney, A. Dhinojwala, M.S. Yeganeh, Molecular origin of solvent resistance of polyacrylonitrile, *Macromolecules* 42 (18) (2009) 7103–7107.
[17] S.K. Nataraj, K.S. Yang, T.M. Aminabhavi, Polyacrylonitrile-based nanofibers—A state-of-the-art review, *Prog. Polym. Sci.* 37 (3) (2012) 487–513.
[18] J. Gao, X.X. Wang, J.S. Zhang, R.L. Guo, Preparation of heat-treated PAN/SiO_2 hybrid hollow fiber membrane contactor for acetylene absorption, *Sep. Purif. Technol.* 159 (2016) 116–123.
[19] Z. Wang, R. Sahadevan, C. Crandall, T.J. Menkhaus, H. Fong, Hot-pressed PAN/PVDF hybrid electrospun nanofiber membranes for ultrafiltration, *J. Membr. Sci.* 611 (2020) 118327.
[20] H.A. Tsai, Y.L. Chen, K.R. Lee, J.Y. Lai, Preparation of heat-treated PAN hollow fiber membranes for pervaporation of NMP/H_2O mixtures, *Sep. Purif. Technol.* 100 (2012) 97–105.
[21] W.B. Li, Z.H. Yang, Q. Meng, C. Shen, G.L. Zhang, Thermally stable and solvent resistant self-crosslinked TiO_2/PAN hybrid hollow fiber membrane fabricated by mutual supporting method, *J. Membr. Sci.* 467 (2014) 253–261.
[22] B. Zhang, D. Wang, Y.H. Wu, Z. Wang, T.H. Wang, J.S. Qiu, Modification of the desalination property of PAN-based nanofiltration membranes by a preoxidation method, *Desalination* 357 (2015) 208–214.
[23] W.B. Li, Z.H. Yang, G.L. Zhang, Q. Meng, Heat-treated polyacrylonitrile (PAN) hollow fiber structured packings in isopropanol (IPA)/water distillation with improved thermal and chemical stability, *Ind. Eng. Chem. Res.* 52 (19) (2013) 6492–6501.
[24] Z.Y. Fu, B.J. Liu, L.H. Sun, H.X. Zhang, Study on the thermal oxidative stabilization reactions and the formed structures in polyacrylonitrile during thermal treatment, *Polym. Degrad. Stab.* 140 (2017) 104–113.
[25] X.H. Qin, Structure and property of electrospinning PAN nanofibers by different preoxidation temperature, *J. Therm. Anal. Calorim.* 99 (2) (2010) 571–575.
[26] S.H. Yen, F.C. Chang, Effects of fiber processing conditions on the yield, carbon content, and diameter of lignosulfonate-based carbon fibers, *BioResources* 11 (4) (2016) 10158–10172.
[27] Gergin, E. Ismar, A.S. Sarac, Oxidative stabilization of polyacrylonitrile nanofibers and carbon nanofibers containing graphene oxide (GO): A spectroscopic and electrochemical study, *Beilstein J. Nanotechnol.* 8 (2017) 1616–1628.
[28] M. Wortmann, N. Frese, A. Mamun, M. Trabelsi, W. Keil, B. Büker, A. Javed, M. Tiemann, E. Moritzer, A. Ehrmann, A. Hütten, C. Schmidt, A. Gölzhäuser, B. Hüsgen, L. Sabantina, Chemical and morphological transition of poly (acrylonitrile)/poly(vinylidene fluoride) blend nanofibers during oxidative stabilization and incipient carbonization, *Nanomaterials* 10 (6) (2020) 1210.
[29] S.S. Homaeigohar, K. Buhr, K. Ebert, Polyethersulfone electrospun nanofibrous composite membrane for liquid filtration, *J. Membr. Sci.* 365 (1–2) (2010) 68–77.
[30] W. Jang, J. Yun, K. Jeon, H. Byun, PVdF/graphene oxide hybrid membranes *via* electrospinning for water treatment applications, *RSC Adv.* 5 (58) (2015) 46711–46717.
[31] R. Wang, Y. Liu, B. Li, B.S. Hsiao, B. Chu, Electrospun nanofibrous membranes for high flux microfiltration, *J. Membr. Sci.* 392–393 (2012) 167–174.
[32] M. Faccini, G. Borja, M. Boerrigter, D. Morillo Martín, S. Martìnez Crespiera, S. Vázquez-Campos, L. Aubouy, D. Amantia, Electrospun carbon nanofiber membranes for filtration of nanoparticles from water, *J. Nanomater.* 2015 (2015) 247471.
[33] X.W. Cao, M.L. Huang, B. Ding, J.Y. Yu, G. Sun, Robust polyacrylonitrile nanofibrous membrane reinforced with jute cellulose nanowhiskers for water purification, *Desalination* 316 (2013) 120–126.